Interface Characterization of the Type II Module Pair from Fibronectin†

Steven P. Smith,‡ Yasuhiro Hashimoto,‡,§ Andrew R. Pickford,‡ Iain D. Campbell,‡,|| and Jörn M. Werner*,‡

Department of Biochemistry, University of Oxford, South Parks Road, Oxford OX1 3QU, U.K., Analytical Research Laboratory, Asahi Chemical Industry, Co. Ltd., Shizuoka 416-8501, Japan, and Oxford Centre for Molecular Sciences, South Parks Road, Oxford OX1 3QT, U.K.

Received February 24, 2000

ABSTRACT: The lone ^{1}F2^{2}F2 modular pair of fibronectin is found in the collagen-binding region. This exclusive localization suggests the ^{1}F2^{2}F2 pair plays an important role in the recognition of collagen. However, no information is currently available about the interaction between the two F2 modules and, thus, the orientation of their putative collagen-binding sites with respect to one another. Comparison of a variety of high-resolution NMR parameters from the F2 modules in isolation and the ^{1}F2^{2}F2 pair was used to establish the extent of interaction between the F2 modules in the pair. Chemical shifts of the F2 modules and the ^{1}F2^{2}F2 pair indicate that the structures of the modules are preserved in the pair and that, with the exception of the covalent linkage, they do not interact. ^{15}N NMR relaxation data identify significant motion occurring in the linker region of the ^{1}F2^{2}F2 pair, and analyses of the anisotropic diffusion properties of the ^{1}F2^{2}F2 pair are consistent with the modules in the F2 pair tumbling independent of one another.

Fibronectin is an extracellular glycoprotein, found as both a soluble dimer in plasma and an insoluble component of the extracellular matrix (*1*). Its roles encompass a variety of physiological events such as embryogenesis, wound healing, cell migration, and the maintenance of tissue integrity. Fibronectin is a mosaic protein composed almost entirely of three types of modules: F1,[1] F2, and F3 (*2*, *3*). These modules are organized into functional domains, which allow the native protein to display a wide array of specific ligand-binding sites across its entire length. An understanding of how these modules associate with one another, to form various binding surfaces, has significant implications for many aspects of extracellular matrix biology.

One important interaction in the extracellular matrix is that between fibronectin and collagen. The collagen-binding region has been localized, on the basis of its affinity for either heat-denatured collagen (gelatin) or isolated collagen α chains, to a 42 kDa proteolytic fragment of fibronectin. It has been shown to comprise the sequential array of modules ^{6}F1^{1}F2^{2}F2^{7}F1^{8}F1^{9}F1 (*4*, *5*). Attempts to further localize this binding site have yielded conflicting results (*6*−*10*). Not all the proteolytic fragments containing the F2 modules were found to bind gelatin, but the exclusive localization of the two F2 modules to this region implicates these modules in gelatin binding. The existence of F2 modules in other gelatin-binding proteins, such as the matrix metalloproteinases (MMP) 2 and 9, provides further evidence for the involvement of F2 modules in gelatin binding (*11*). Furthermore, recombinant expression of F2 modules from these MMPs has produced fragments with high affinity for gelatin (*9*, *12*, *13*), whereas recombinant MMP lacking F2 modules was found to lack gelatin-binding activity (*14*, *15*).

Solution structures of the F2 modules PDC-109b from PDC-109 (*16*), the ^{1}F2 (*17*) and ^{2}F2 (*18*) modules from fibronectin, and the ^{1}F2 module from MMP2 (*19*) have been determined by high-resolution nuclear magnetic resonance (NMR). The consensus topology consists of two double-stranded antiparallel β-sheets, oriented almost perpendicular to each other. This arrangement encloses a cluster of conserved aromatic amino acid residues, some of which form an exposed hydrophobic surface. Recent binding studies using a synthetic collagen consensus peptide, $(Pro\text{-}Pro\text{-}Gly)_6$, have identified a ligand-binding site on one face of the second F2 module of MMP2 comprising Phe21, Trp40, Tyr47, Tyr53, and Phe55 (*19*). Interestingly, the crystal structure of human proMMP2 (*20*), containing three F2 modules, indicated that these F2 binding sites are oriented to face in opposite directions, in contrast to a previously suggested model, with a continuous binding motif. The second F2 module also appears to have little, if any, interaction with either the first or the third F2 modules.

Since the structure determination of isolated modules has elucidated potential interaction surfaces, the study of larger fragments is now required to obtain information about their

† S.P.S. is a recipient of a Burroughs Wellcome Fund Hitchings-Elion Fellowship. This research was supported by the Wellcome Trust, the Biotechnology and Biological Sciences Research Council, the Medical Research Council, and the Engineering and Physical Sciences Research Council. This is a contribution from the Oxford Centre of Molecular Sciences.

* To whom correspondence should be addressed. Telephone: +44 (0)1865 275 720. Fax: +44 (0)1865 275 253. E-mail: jmw@bioch.ox.ac.uk.

‡ University of Oxford.

§ Asahi Chemical Industry, Co. Ltd.

|| Oxford Centre for Molecular Sciences.

[1] Abbreviations: F1, fibronectin type I module; F2, fibronectin type II module; F3, fibronectin type III module; MMP, matrix metalloproteinase; NMR, nuclear magnetic resonance; HPLC, high-performance liquid chromatography; GlcNAc, *N*-acetylglucosamine; pH*, pH unadjusted for deuterium; GE, General Electric; NOE, nuclear Overhauser effect; CPMG, Carr−Purcell−Meiboom−Gill; CSA, chemical shift anisotropy; T_1, longitudinal relaxation time constant; T_2, transverse relaxation time constant; HSQC, heteronuclear single-quantum coherence; δ, chemical shift.

10.1021/bi000427i CCC: $19.00
Published on Web 06/30/2000

spatial arrangement and about how they interact with collagen. Modeling studies of the ^{1}F2^{2}F2 pair from fibronectin suggested that the two modules do not interact tightly and have no preferred orientation with respect to one another (*18*). This observation precluded the notion of a continuous collagen-binding site (*18*); however, experimental evidence regarding the nature of the interface of the ^{1}F2^{2}F2 pair from fibronectin has not yet been obtained.

New NMR techniques have recently been employed to provide information about long-range order in multidomain proteins. These methods include the use of magnetically oriented dilute liquid crystalline media (*21, 22*), magnetically aligned molecules (*23, 24*), and the dependency of ^{15}N relaxation on anisotropic diffusion (*25*−*27*). All of these methods rely on a defined global coordinate system, but the effects of averaging of the global axis system, caused by interdomain motion, are not well understood.

Comparison of NMR-derived structural and dynamic information of isolated modules with multimodule fragments provides an elegant method for probing the extent of module−module interactions. In this work, we use chemical shift and backbone relaxation rate information, derived from the isolated ^{1}F2 and ^{2}F2 modules as well as the ^{1}F2^{2}F2 pair, to study the extent to which these two modules interact. Our results suggest that the structures of the F2 modules are essentially unchanged when covalently linked to one another and that the ^{1}F2^{2}F2 pair lacks a well-defined interface; this allows them to tumble essentially independently of one another.

EXPERIMENTAL PROCEDURES

Protein Expression and Purification. Unlabeled and uniformly ^{15}N-labeled ^{1}F2^{2}F2 module pairs, corresponding to residues 315−374 of mature human fibronectin, were produced by recombinant expression from the methylotrophic yeast *Pichia pastoris* as outlined by Bright et al. (*28*). Purification of the recombinant protein followed the procedures used for the ^{1}F2 module (*17*) with two additional steps preceding the final reversed-phase HPLC step. An affinity chromatography step on gelatin-Sepharose 4B (Amersham Pharmacia Biotech) was followed by cleavage of the high-mannose sugar on the ^{2}F2 module using endoglycosidase H_f (New England Biolabs), leaving a single *N*-acetylglucosamine (GlcNAc) attached to residue Asn85. Uniformly ^{15}N-labeled ^{1}F2 and ^{2}F2 were expressed as described above and purified as reported previously (*17, 18*).

NMR Spectroscopy and Data Analysis. NMR samples of unlabeled ^{1}F2^{2}F2 contained 1.0 mM protein in 0.6 mL of 100% D_2O (pH* 6.0), and samples of uniformly labeled [^{15}N]^{1}F2, [^{15}N]^{2}F2, and [^{15}N]^{1}F2^{2}F2 contained 1.2 mM protein in 0.6 mL of a 90% H_2O/10% D_2O mixture at pH 6.0. All NMR spectra were recorded on home-built GE-Omega spectrometers fitted with triaxial gradient, triple-resonance probes. Pulsed field gradients were employed for coherence selection and water suppression (*29*). ^{15}N decoupling during acquisition was carried out using a 833 Hz GARP1 decoupling field (*30*). Experiments were carried out at 25 °C. For the assignment of the ^{1}F2^{2}F2 module pair, the following spectra were acquired. A two-dimensional (2D) ^{1}H−^{1}H Hartmann−Hahn (HOHAHA) spectrum (42 ms mixing time) (*31*), with a 7 kHz DIPSI2 mixing sequence, and a 2D ^{1}H−^{1}H NOESY spectrum (125 ms mixing time) (*32*) were acquired on unlabeled ^{1}F2^{2}F2 at 17.6 T with acquisition times of 256.0 ms in t_2 and 42.0 ms in t_1; a three-dimensional (3D) ^{15}N-edited TOCSY-HSQC spectrum (42 ms mixing time) (*33*) and a 3D ^{15}N-edited NOESY-HSQC spectrum (125 ms mixing time) (*33*) were collected at 11.7 T with acquisition times of 20.0 ms in t_2 (^{1}H), 30.7 ms in t_1 (^{15}N), and 51.2 ms in t_3 (^{1}H). ^{1}H−^{15}N HSQC spectra (*29*) acquired on the isolated F2 modules and the ^{1}F2^{2}F2 pair were collected at 11.7 T with acquisition times of 128.0 ms in t_2 (^{1}H) and 130.0 ms in t_1 (^{15}N).

^{15}N T_1, ^{15}N T_2, and {^{1}H}−^{15}N NOE data were measured at 11.7 T with acquisition times of 117.0 ms in t_1 (^{15}N) and 128.0 ms in t_2 (^{1}H) using previously described methods (*34*). Transverse relaxation time constants (T_2) were measured using a spin−echo sequence with a CPMG delay of 570 μs. Dipolar and chemical shift anisotropy (CSA) cross correlation was removed by application of proton 180° pulses every 5 ms (T_1) and in the middle of the basic CPMG block (T_2) (*35, 36*). Inaccuracies in T_2 measurements associated with sample heating were reduced by including a train of ^{15}N refocusing pulses and delays trailing the pulse sequence such that the total number of refocusing pulses was the same in each T_2 experiment (*37*). Heating was assessed by comparison of the H^N and ^{15}N chemical shift changes in the T_2 spectra with the minimum and maximum number of ^{15}N refocusing pulses. Provided each experiment was preceded by 15 min of dummy scans, peak intensities could be reproduced reliably. Each series of T_1 and T_2 measurements consisted of eight autocorrelation spectra with increasing ^{15}N relaxation delays, including one repeat experiment. Delays were chosen to sample approximately the whole intensity decays, with the largest delay being at least 1.5 times the average relaxation time constant.

Pairs of ^{1}H-detected {^{1}H}−^{15}N heteronuclear NOE experiments with and without NOE were carried out using the above acquisition parameters. ^{1}H saturation in the NOE experiment was effected by means of a train of 120° flip-angle pulses at 10 ms intervals for 2.5 s. The data sets used for the analysis were acquired using 1.2 mM samples. Control spectra of the ^{15}N T_1, ^{15}N T_2, and {^{1}H}−^{15}N NOE were also collected on 0.6 mM samples, to ensure that aggregation was not affecting the relaxation time constants.

Homonuclear HOHAHA and NOESY spectra were processed as described previously (*17*). The 3D TOCSY-HSQC and NOESY-HSQC data were processed using a linear prediction in t_1 from 96 to 128 points, prior to apodization, using a Lorentzian−Gaussian function in t_2 and a Kaiser function in t_1 and t_3. The ^{15}N T_1, ^{15}N T_2, and {^{1}H}−^{15}N NOE data were processed with mild resolution enhancement to optimize resolution while maintaining a good signal-to-noise ratio using Felix 2.3 (Biosym, Inc., San Diego, CA). Overlapped resonances in the ^{15}N T_1, ^{15}N T_2, and {^{1}H}−^{15}N NOE spectra were not analyzed in detail. T_1 and T_2 relaxation time constants were determined by least-squares fits of the resonance intensities to the two-parameter exponential decay. Errors were determined from the standard deviations of differences in the peak intensities in the spectra, which were recorded in duplicate (*38*). The heteronuclear NOE effect was calculated as the ratio of resonance intensities in the spectra recorded with and without the NOE. Errors in the heteronuclear NOE were estimated from the signal-to-noise

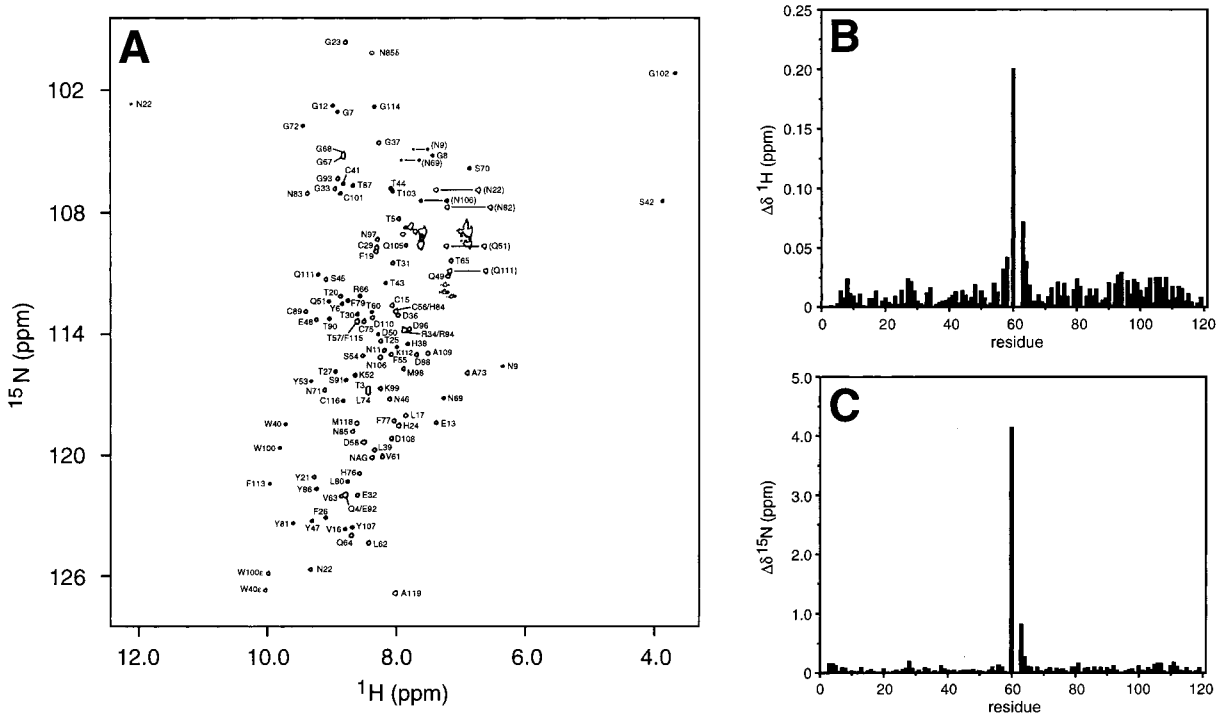

FIGURE 1: Chemical shift comparison of isolated F2 modules with the ^{1}F2^{2}F2 pair. (A) ^{1}H−^{15}N HSQC spectrum of 1.2 mM ^{1}F2^{2}F2 at pH 6.0 and 25 °C recorded at 11.7 T. Backbone amide proton resonances are labeled with the one-letter amino acid code followed by the position in the sequence. Assigned NH_2 side chain resonances are connected by lines, and the corresponding assignments are in parentheses. Gray peaks are folded resonances. (B) The H^N chemical shift difference between the F2 modules in isolation and in the ^{1}F2^{2}F2 pair. (C) The ^{15}N chemical shift difference between the F2 modules in isolation and in the ^{1}F2^{2}F2 pair.

ratio of each spectrum.

Modeling of Relaxation Data. The values of the ^{15}N relaxation time rate constants were derived assuming dipolar and CSA relaxation using the usual fundamental constants together with 1.02 Å for the NH bond length. The chemical shift anisotropy was assumed to be −170 ppm and to be collinear with the dipolar tensor (*39*). The principal axes D_x, D_y, and D_z of the diffusion tensor **D** were determined by global least-squares fits of the T_1/T_2 ratios derived from the spectral density functions of a diffusing particle to the experimental values (*40*−*42*). Three models were tested: a sphere [$D_x = D_y = D_z$, $D = (D_x + D_y + D_z)/3$], a symmetric top [$D_{||} = D_z$, and $D_\perp = (D_x + D_y)/2$], and a fully asymmetric tensor ($D_x \neq D_y \neq D_z$) (*43*).

In the case of a symmetric top, the spectral density function is given by

$$J(\omega) = \sum_{k=1,2,3}^{} A_k[\tau_k/(1 + \omega^2\tau_k^2)]$$

where $A_1 = (1.5 \cos^2 \theta - 0.5)^2$, $A_2 = 3 \sin^2 \theta \cos^2 \theta$, and $A_3 = 0.75 \sin^4 \theta$, and correlation times $\tau_1 = 6D_\perp^{-1}$, $\tau_2 = (D_{||} + 5D_\perp)^{-1}$, and $\tau_3 = (4D_{||} + 2D_\perp)^{-1}$. The analysis was performed with the program modelfree4 (kindly provided by A. G. Palmer, III, Columbia University, New York, NY) and programs written in house. The diffusion tensors were estimated by minimizing χ^2 in a grid search method followed by least-squares fitting:

$$\chi^2 = \sum^{i}\{[(T_{1i}/T_{2i})_{calc} - (T_{1i}/T_{2i})_{obs}]^2/\sigma_i^2\}$$

where σ_i is the experimental uncertainty of the T_{1i}/T_{2i} ratio of each included residue. Model comparisons were performed by using the *F* test and by calculation of the probability *Q* of obtaining a given *F* value by chance (*44*).

RESULTS AND DISCUSSION

Resonance Assignment of the ^{1}F2^{2}F2 Module Pair and Comparison with ^{1}F2 and ^{2}F2. Backbone amide chemical shift assignments of the ^{1}F2^{2}F2 pair were obtained using sequential $d_{\alpha N}$ and d_{NN} connectivities from an ^{15}N-edited NOESY-HSQC spectrum. A ^{1}H−^{15}N HSQC spectrum of the ^{1}F2^{2}F2 modular pair is shown in Figure 1A with 110 of the 114 expected backbone amide proton (H^N) resonances identified. In addition, seven of the possible 18 pairs of side chain H^N resonances were assigned unambiguously as were the resonances corresponding to the side chain of Asn85$^{N\delta}$ and the H^N of the Asn85-N-linked GlcNAc carbohydrate. Of the eight residues not observed in the spectrum, four were proline residues (Pro14, Pro18, Pro78, and Pro117), while Ala1, Val2, Gln35, and Arg95 all appeared to undergo fast exchange with solvent at pH 6.0. Similar results were observed for the F2 modules in isolation, with Val1 and Leu2 of the ^{2}F2 module also undergoing fast solvent exchange. The spectrum is well-resolved with only a small number of overlapping resonances. Specifically, the resonances of Gln4 and Glu92, Arg34 and Arg94, Thr57 and Phe115, and Cys56 and His84 had degenerate amide proton and nitrogen chemical shifts. The backbone H^N chemical shifts of Ser42 and Gly102 are shifted upfield, identical to those observed for the F2 modules in isolation (*17*, *18*), and can attributed to ring current effects caused by proximal aromatic side chains (Phe19 and Phe79) found in the core of the individual F2 modules.

Since chemical shift is very sensitive to changes in the local environment, it can be used extensively to monitor

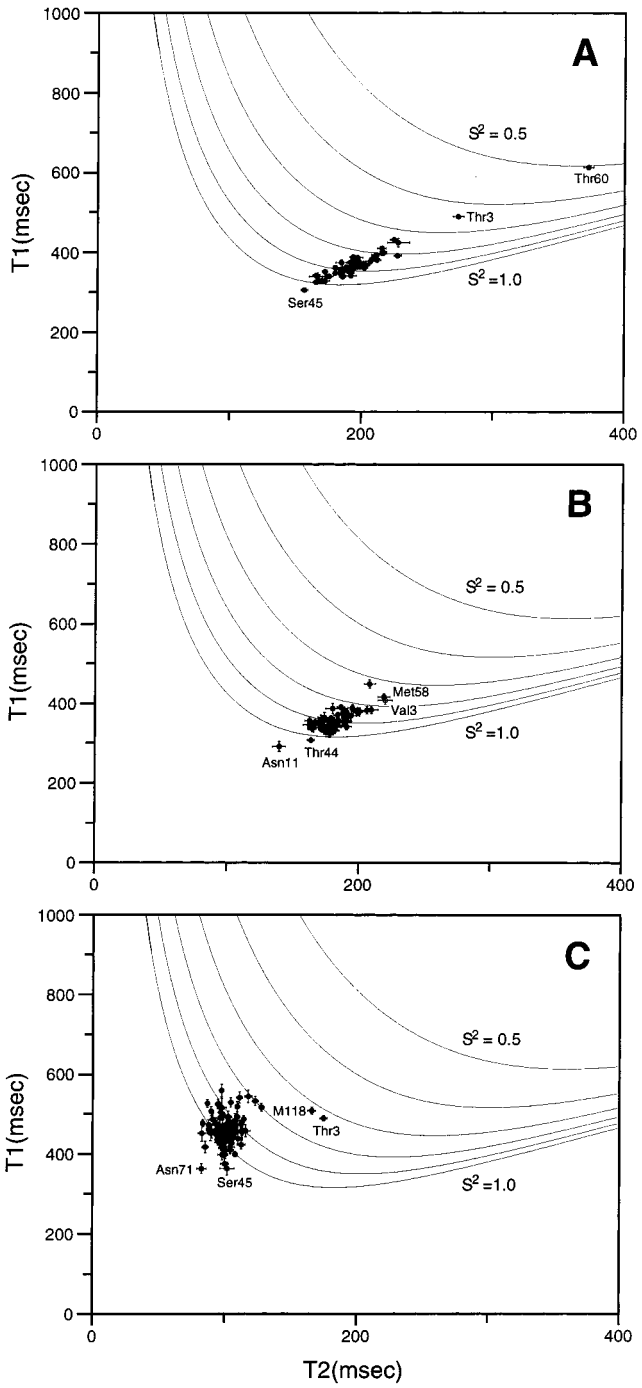

FIGURE 2: Backbone ^{15}N relaxation rates for the isolated F2 modules and the ^{1}F2^{2}F2 module pair measured at 11.7 T. T_2 vs T_1 plot of (A) the 56 residues from the ^{1}F2 module, (B) the 53 residues from the ^{2}F2 module, and (C) the 99 residues from the ^{1}F2^{2}F2 module pair. Outlying residues are labeled appropriately. The continuous lines are calculated T_1 and T_2 values as a function of correlation time and the order parameter, S^2, using the isotropic Lipari−Szabo model (*58*). Curves with values of S^2 equaling 0.5, 0.6, 0.7, 0.8, 0.9, and 1.0 are shown with the highest and lowest values labeled accordingly.

protein−protein interactions. Comparison of the backbone H^N and ^{15}N chemical shifts of the ^{1}F2^{2}F2 pair with those of the isolated ^{1}F2 and ^{2}F2 modules (panels B and C of Figure 1, respectively) indicate, with the exception of Thr60 at the C-terminus of the ^{1}F2 module and Val3 at the N-terminus of the ^{2}F2 module, an absence of significant chemical shift differences. The chemical shift differences observed for

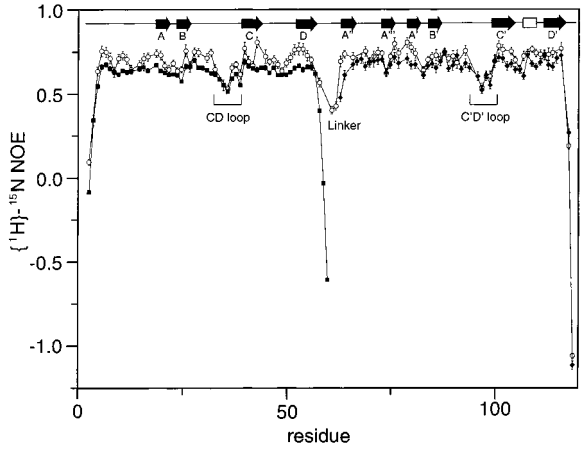

FIGURE 3: {^{1}H}−^{15}N NOE for the isolated F2 modules and the ^{1}F2^{2}F2 module pair. The data for ^{1}F2 and ^{2}F2 are represented by filled squares and filled diamonds, respectively. The data for the ^{1}F2^{2}F2 module pair are represented by open circles. The secondary structure elements are depicted above the data with arrows representing β-strands, open boxes as helices, and thin lines as loop structures. The β-strands are labeled A−D in the ^{1}F2 module and A′−D′ in the ^{2}F2 module. The positions of the linker and the loops comprising residues 34−39 in the ^{1}F2 (termed the CD loop) and ^{2}F2 (termed the CD′ loop) modules are indicated.

Thr60 and Val3 are expected to arise because of a change in the covalent peptide linkage between Thr60 of ^{1}F2 and Val1 of ^{2}F2. The absence of chemical shift changes for the remainder of the residues in the F2 modules suggests that backbone conformations of the two modules in the pair are not perturbed and that there is no apparent long-range interaction between the ^{1}F2 and ^{2}F2 modules in the pair. Analogous observations have been made in studies of the Abl SH(32) module pair (*45*) and an immunoglobulin-like module pair from titin (*46*). In contrast to these results, chemical shift changes were observed in other fibronectin module pairs, where module−module interactions have been identified. In the ^{6}F1^{1}F2 pair of fibronectin, a large backbone chemical shift change, in Ser69 of the ^{1}F2 module, is induced by the presence of the preceding ^{6}F1 module (*47*), while residues of ^{10}F3 at the interface of the ^{9}F3^{10}F3 module pair of fibronectin display changes in chemical shift when compared to ^{10}F3 in isolation (*48*).

The ^{15}N-edited 3D NOESY-HSQC and homonuclear 2D NOESY spectra allowed for the complete assignment of side chain resonances of the ^{1}F2^{2}F2 pair and the assignment of >95% of short-, medium-, and long-range NOEs. All NOEs previously observed in the two isolated F2 modules (*17*, *18*) were identified, indicating that the structures of the two modules have not been significantly altered by the covalent linkage of a second F2 module. In addition, no linker−module NOEs or module−module NOEs could be identified during the assignment procedure. In contrast, more than 40 linker−module and four module−module NOEs were identified in the ^{9}F3^{10}F3 module pair which displayed an extended structure with some flexibility at the modular interface (*49*). The absence of chemical shift perturbation and the lack of intermodule NOEs in the ^{1}F2^{2}F2 module pair, in conjunction with the flexibility observed in the ^{9}F3^{10}F3 module interface where a number of linker NOEs have been identified, strongly suggest that a stable interface is not formed between the F2 module pair.

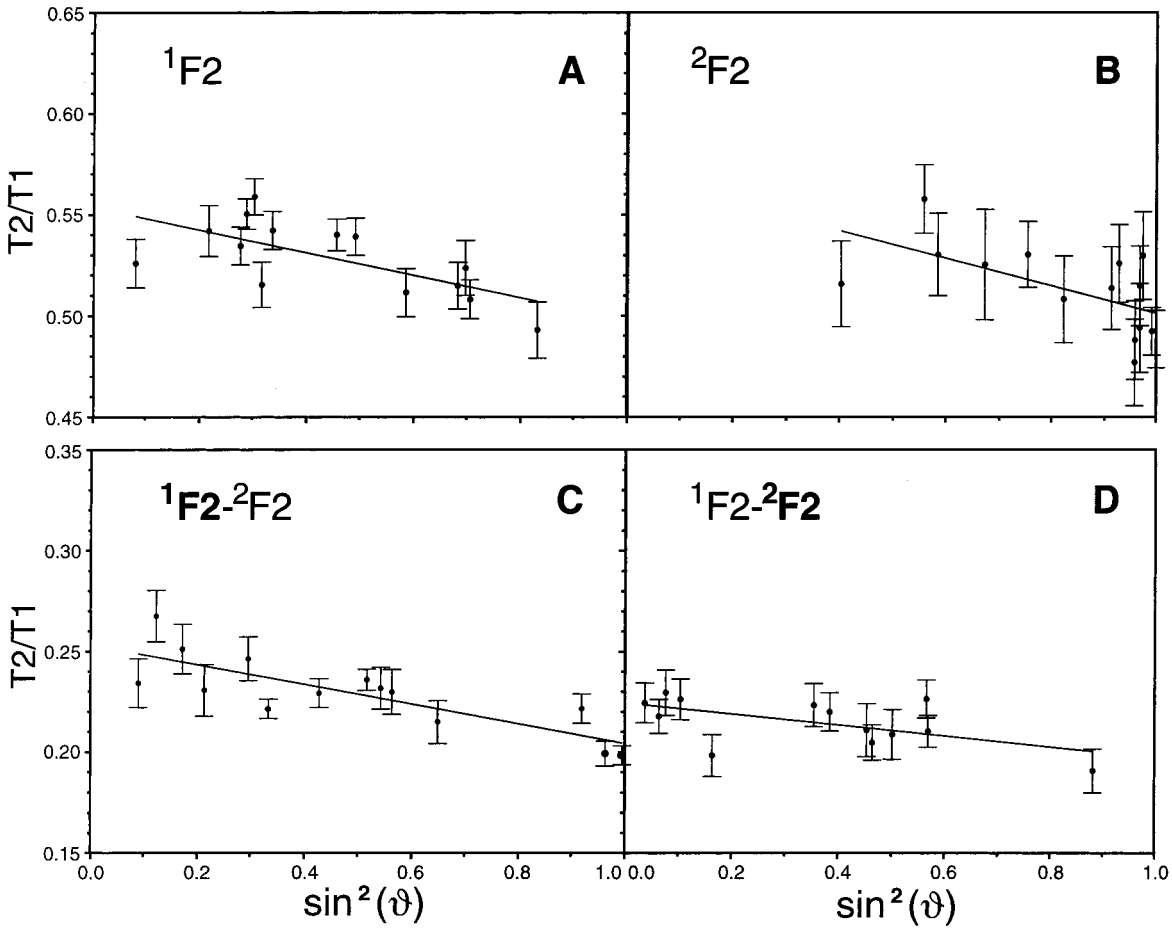

FIGURE 4: Dependence of the $(T_1/T_2)^{-1}$ ratios on the angle θ between the NH bond vector and the unique axis of the diffusion tensor. Diffusion anisotropy of (A) ^{1}F2 in isolation, (B) ^{2}F2 in isolation, (C) ^{1}F2 (bold) in the ^{1}F2^{2}F2 pair, and (D) ^{2}F2 (bold) in the ^{1}F2^{2}F2 pair. The straight line is obtained by linear regression, and the slope is a linear function of the axial ratio of the diffusion tensor.

Relaxation Data. To further characterize the mobility of the two modules in the ^{1}F2^{2}F2 pair, longitudinal ^{15}N T_1 and transverse ^{15}N T_2 relaxation time constants and the steady-state $\{^1H\}-^{15}N$ NOE were measured at 11.7 T for the isolated ^{1}F2 and ^{2}F2 modules and the ^{1}F2^{2}F2 module pair. Reliable quantitation of peak intensities was possible for 56 of the expected 57 H^N backbone resonances in the ^{1}F2 module, 53 of the expected 56 H^N backbone resonances in the ^{2}F2 module, and 99 of the expected 114 H^N backbone resonances in the ^{1}F2^{2}F2 module pair.

The experimental T_1 and T_2 values are plotted against one another in Figure 2 for the two F2 modules and the F2 module pair. The average T_1 and T_2 values for ^{1}F2, ^{2}F2, and ^{1}F2^{2}F2 are 373 and 198 ms, 370 and 193 ms, and 461 and 103 ms, respectively. Measurements of relaxation time constants on a ^{1}F2^{2}F2 sample with half the concentration yielded results very similar to those for the 1.2 mM sample, suggesting that unspecific aggregation is insignificant. Very little deviation from the above average values is seen for all three molecules, suggesting that, in each case, the relaxation properties of the molecule are governed by the overall diffusion tensor. A small number of residues at the N- and C-termini of ^{1}F2 (Thr3 and Thr60), ^{2}F2 (Val3 and Met58), and ^{1}F2^{2}F2 (Thr3 and Met118) were found to have smaller T_1/T_2 ratios, indicating increased mobility in these regions. These observations are consistent with those previously seen for mobile loops and tails of a variety of other proteins (*25*, *50*−*53*). The T_2 values of Ser45 from isolated ^{1}F2 and Asn11 and Thr44 from isolated ^{2}F2 are smaller than predicted by overall diffusion (Figure 2A,B), implying that these residues undergo chemical exchange. In the pair, the same residues exhibit depressed T_2 values (Figure 2C). In addition, Val61 and Leu62 in the linker region exhibit larger than average T_1 and T_2 values (520 and 129 ms, and 536 and 124 ms, respectively) indicative of increased mobility compared to residues in the core region of the F2 modules.

The $\{^1H\}-^{15}N$ NOE values for the F2 modules in isolation and the ^{1}F2^{2}F2 pair are plotted in Figure 3. The average values (0.647 for ^{1}F2, 0.675 for ^{2}F2, and 0.730 for ^{1}F2^{2}F2), derived using residues in regions with secondary structure, imply that the modules are well-ordered. Further, the average $\{^1H\}-^{15}N$ NOE values for each F2 module in the pair are the same, within experimental error, indicating that their high-frequency dynamic behavior is similar. Significantly reduced NOEs are observed for residues in the N- and C-termini of ^{1}F2 (Val3−Thr5 and Asp58−Thr60), ^{2}F2 (Val3, Gln4, Met58, and Ala59), and ^{1}F2^{2}F2 (Val3, Met118, and Ala119). Reduced values were also found for the loop region between β-strands C and D comprising residues 34−39 in the ^{1}F2 (CD loop) and ^{2}F2 (C′D′ loop) modules. The same trend is also observed in the ^{1}F2^{2}F2 pair, showing that these loops maintain their mobility in each F2 partner. A significant reduction in NOE values is also noted for residues Met58, Val61, and Leu62 in the linker region of the ^{1}F2^{2}F2 pair, indicating the presence of sub-nanosecond time scale motion for these residues. These results, which suggest a mobile

Table 1: Diffusion Parameters for ^{1}F2, ^{2}F2, and ^{1}F2^{2}F2[a]

	$(6D)^{-1}$	$2D_{zz}/(D_{xx}+D_{yy})$	D_{xx}/D_{yy}	θ[b]	ϕ[b]	ψ[b]	χ^2	Q_1[c]	Q_2[c]
^{1}F2									
isotropic	3.32						39.7		
axially symmetric									
prolate[d]	3.39	1.31		78	56		24.4		
oblate[d]	3.43	0.73		69	146		21.8	5.8×10^{-2}	
asymmetric	3.40	0.71	0.78	57	142	−2	18.3		0.66
^{2}F2									
isotropic	3.47						22.2		
axially symmetric									
prolate[d]	3.44	1.20		60	−23		15.6		
oblate[d]	3.33	0.67		26	166		11.1	1.8×10^{-2}	
asymmetric	3.37	0.65	0.92	25	174	76	10.0		0.86
^{1}F2 in the ^{1}F2^{2}F2 pair									
isotropic	7.11						73.8		
axially symmetric									
prolate[d]	7.33	1.84		10	45		31.6		
oblate[d]	7.13	0.73		81	107		24.0	2.1×10^{-2}	
asymmetric	7.12	0.67	1.37	97	90	7	20.8		0.76
^{2}F2 in the ^{1}F2^{2}F2 pair									
isotropic	7.22						14.9		
axially symmetric									
prolate[d]	7.33	1.12		−24	40		12.7		
oblate[d]	7.44	0.85		97	157		10.6	0.39	
asymmetric	7.47	0.83	0.91	98	154	−46	10.4		0.99

[a] Parameters were obtained by fitting experimental T_1/T_2 values to the averaged minimized structures of ^{1}F2 and ^{2}F2. [b] Euler angles of the principle axes of the diffusion tensor in the principal axis frame a common molecular frame. [c] Q_1 was calculated for the comparison of the isotropic and axially symmetric models. Q_2 was calculated for the comparison of the axially asymmetric (oblate) and asymmetric models. [d] Fits were carried out assuming a prolate $[2D_{zz}/(D_{xx}+D_{yy}) > 1.0]$ or an oblate $[2D_{zz}/(D_{xx}+D_{yy}) < 1.0]$ diffusion tensor.

linker region in the ^{1}F2^{2}F2 pair, are consistent with results observed for linker regions in a number of proteins, where few or no intermodule NOEs were observed, including calmodulin (*50*) and the ^{1}F1^{2}F1 (*54*) and ^{6}F1^{1}F2 (*55*) module pairs of fibronectin. Unlike calmodulin, the short five-residue linker would initially suggest limited flexibility between the two F2 modules, as seen for the ^{9}F3^{10}F3 module pair (*49*). However, a previous conformational search study on the ^{1}F2^{2}F2 module pair using rigid F2 modules with an unconstrained linker showed that the relative orientation of one F2 module is only limited by the excluded volume of its respective partner (*18*). The absence of linker−module and module−module NOEs supports the conformational search study and suggests that the residues in the linker are not constrained to a specific conformation, allowing the modules to explore a wide range intermodule orientations.

Estimation of Rotational Diffusion Tensors and Rotational Correlation Times. The degree of coupling between the two F2 modules in the ^{1}F2^{2}F2 pair was investigated by comparing the diffusion anisotropies of the F2 modules in isolation with those in the ^{1}F2^{2}F2 module pair in a fashion similar to that of Fushman et al. (*27*). The T_1 and T_2 relaxation time constants of the isolated F2 modules and those of the ^{1}F2^{2}F2 pair were analyzed using an isotropic, axially symmetric and fully asymmetric diffusion tensor. Since analysis of the chemical shifts indicated that the structures of the F2 modules were not significantly altered upon covalent linkage with the respective partner, the average minimized structures of the individual F2 modules (*17*, *18*) were used to fit the relaxation data of the module in isolation and in the pair. The analysis was performed on a common set of residues located in secondary structure and with angular order parameters of the backbone dihedral angle ϕ of >0.94, namely, β-strands A−D, with the exception of Leu39, Trp40, and Ala109. The results are shown in Figure 4 and summarized in Table 1. As expected from the average T_1 and T_2 values, the isotropic correlation times of the isolated ^{1}F2 ($\tau_m = 3.3$ ns) and ^{2}F2 ($\tau_m = 3.4$ ns) modules are typical of small globular 6.8 kDa proteins (*56*). Inspection of the Q_1 values in Table 1 shows that incorporation of anisotropic diffusion yields significantly better interpretation of the data for axially symmetric diffusion tensors. As can be seen from the large Q_2 values, however, extension of the interpretation to a fully asymmetric model does not yield significant improvement. Within the axially symmetric model, the oblate diffusion tensors consistently fitted the data better than the prolate, suggesting that the F2 modules resemble a disk-like conformation rather than a cigar-like shape, which was observed for the ^{9}F3^{10}F3 module pair of mouse fibronectin (*49*). The axial ratios between the unique axes and the two degenerate axes in the isolated ^{1}F2 and ^{2}F2 modules are 0.73 and 0.67, respectively. If θ denotes the angle of the NH bond vector with the unique axis of the diffusion tensor, then for an oblate diffusion tensor one expects the $(T_1/T_2)^{-1}$ ratios to be larger for small θ values and smaller when θ is equal to 90°. A plot of these ratios as a function of $\sin^2\theta$ (*49*) yields a straight line with a negative slope as seen in Figure 4. In the case of the ^{1}F2 module, the angles are well sampled, making the estimate of the anisotropy more robust than in the case of the ^{2}F2, where there are fewer residues at small angles (Figure 4B). However, incorporation of additional residues, from secondary structure elements unique to ^{2}F2 in the fit, improved the sampling of the angles and decreased the axial ratio from 0.67 to 0.83 without changing the orientation of the diffusion tensor. Accordingly, the results do not critically depend on the choice of data set. Hence, the relaxation data of the isolated F2 modules suggest that both molecules have oblate diffusion tensors. This is in good agreement with their overall pancake-like shape (Figure 5).

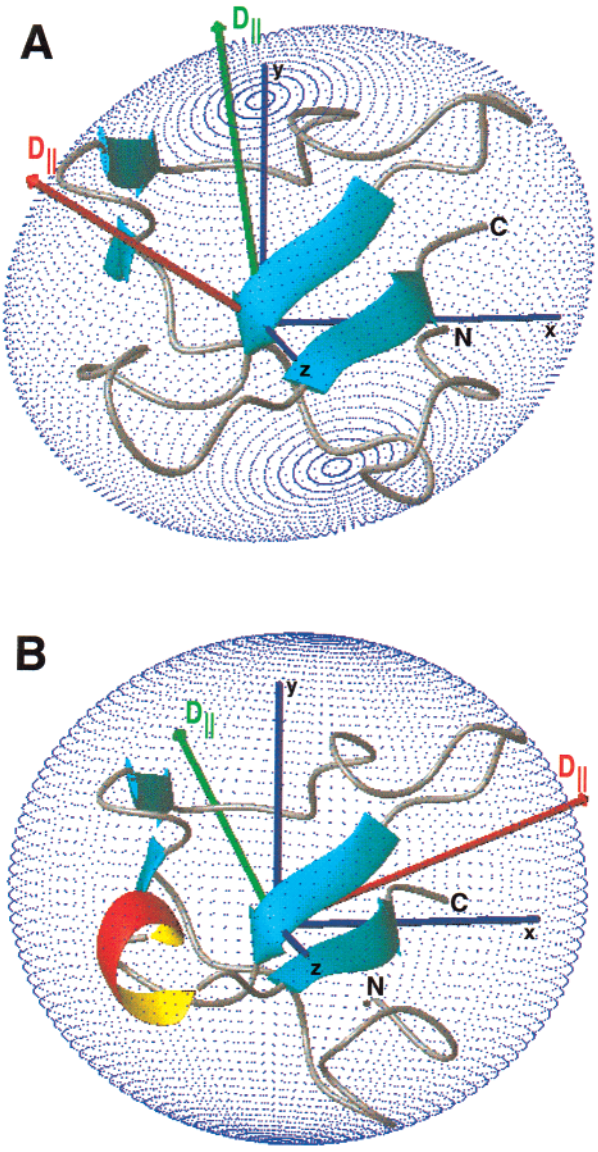

FIGURE 5: Representation of the unique axes ($D_{||}$) of the diffusion tensors in a common molecular frame superimposed on the ribbon diagrams for residues 3−57 of the respective modules. Unique axes ($D_{||}$) of the diffusion tensors of (A) the ^{1}F2 module in isolation and in the pair and (B) the ^{2}F2 module in isolation and in the pair are shown as red and green arrows, respectively. The approximate shapes of the molecules are depicted as dotted ellipsoids. β-Strands are shown as cyan arrows, and the helical turn is colored red. The N- and C-termini are labeled N and C, respectively, and the axes of the inertia frame *x*, *y*, and *z*, respectively. The figure was produced using MolMol (*59*).

The relaxation time constants of the ^{1}F2^{2}F2 pair were analyzed for each module individually. The diffusion properties of ^{1}F2 and ^{2}F2 in the pair were obtained by fitting diffusion tensors to the relaxation time constants of the respective modules (Table 1). The isotropic correlation times of ^{1}F2 and ^{2}F2 in the pair are 7.1 and 7.2 ns, respectively. Together with the absence of significant differences in the heteronuclear NOEs (see above), the data suggest that both their high- and low-frequency behavior are very similar. Furthermore, the correlation times are essentially the sums of the correlation times of the isolated modules, as expected for a molecule with twice the mass of the isolated modules. In contrast, studies on the two-domain molecules calcium-bound calmodulin (*50*), the amino-terminal fragment of the urokinase-type plasminogen activator (*51*), and the HIV-1 nucleocapsid protein (*53*) all showed that their respective domains had different intrinsic rotational correlation times. More detailed analysis of the relaxation data for ^{1}F2 revealed that the diffusion tensor of this module is oblate with the same axial ratio as the single ^{1}F2 module (Table 1 and Figure 4). In the case of ^{2}F2, the data indicate a similar trend; the significance levels for the anisotropic interpretation are, however, not as high. While an oblate diffusion tensor with an axial ratio of 0.85 fits the relaxation data of ^{2}F2 in the pair better than a prolate or an isotropic model, there remains a 40% probability that the improvement over the isotropic model was obtained by chance (Table 1). In this analysis, the axial ratios of the ^{2}F2 module, in isolation and as part of the pair, are found to be different. However, this apparent difference is removed by better sampling of the angles with respect to the unique axis in the isolated ^{2}F2 module (see above).

Comparisons of orientations of the unique axes ($D_{||}$) of the diffusion tensors with respect to a common molecular frame of the respective modules are shown in Figure 5. The unique axes ($D_{||}$) of both modules are reoriented to some extent in the presence of their respective partner (red to green arrows in Figure 5). The azimuth (φ) and polar angle (θ) change by about 40° and 12° and by 9° and 61° in ^{1}F2 and ^{2}F2, respectively (Table 1 and Figure 5). Hence, the principal axes ($D_{||}$ and $D_{\perp}$) of the diffusion tensors for the isolated modules and those of the diffusion tensors in the pair do not align. If one were to assume a single diffusion tensor for the ^{1}F2^{2}F2 pair, implying a well-defined module−module orientation, the axial ratio of this diffusion tensor would, in general, be different from the axial ratios of the individual diffusion tensors. However, the relaxation data show that the axial ratios of the principal axes of the diffusion tensors remain the same (Table 5). Accordingly, we interpret the observation that the axial ratios of the diffusion tensors of the F2 modules remain unchanged in the presence of their respective partners as an indication that motional averaging is occurring between the two modules.

The comparisons of NMR-derived parameters from isolated F2 modules with those from the ^{1}F2^{2}F2 module pair have thus established that the pair is uncoupled. Lack of specific module−module association in the ^{1}F2^{2}F2 pair has been shown by lack of chemical shift changes, the absence of linker−module and module−module NOEs, and diffusion anisotropy analysis of ^{15}N relaxation measurements.

The extent of module−module interactions in fibronectin has been shown to have significant biological implications. For example, while some flexibility is present at the interface of the ^{9}F3^{10}F3 module pair, interactions restrict the relative orientations of the modules and thereby enhance the cell attachment activity of the module pair (*48*, *49*, *57*). In contrast, a biological implication of the uncoupled nature of the F2 modules is that a well-structured interaction surface for collagen does not exist in this isolated fibronectin fragment. This may allow fibronectin to adapt the collagen-binding surfaces of the F2 modules to the collagen recognition sites. Alternatively, the presence of additional fibronectin modules in the intact protein may stabilize a preferred orientation of the F2 modules, generating a well-defined recognition site for collagen. To address this question, larger

fibronectin fragments are currently being studied in our laboratory.

ACKNOWLEDGMENT

We thank Christina Redfield for providing the initial Fortran routine for fitting the fully asymmetric diffusion tensor, Robin Alpin for help concerning mass spectrometry, and Jonathan Boyd and Nick Soffe for NMR technical support.

SUPPORTING INFORMATION AVAILABLE

One table containing ^{15}N relaxation times and {^{1}H}−^{15}N NOE ratios for ^{1}F2, ^{2}F2, and ^{1}F2^{2}F2. This material is available free of charge via the Internet at http://pubs.acs.org.

REFERENCES

1. Hynes, R. O. (1990) *Fibronectin*, Springer-Verlag, Berlin.
2. Potts, J. R., and Campbell, I. D. (1994) *Curr. Opin. Cell Biol. 6*, 648−655.
3. Potts, J. R., and Campbell, I. D. (1996) *Matrix Biol. 15*, 313−320.
4. Hahn, L., and Yamada, K. (1979) *Proc. Natl. Acad. Sci. U.S.A. 76*, 1160−1163.
5. Guidry, C., MIller, E. J., and Hook, M. (1990) *J. Biol. Chem. 265*, 19230−19236.
6. Owens, R. J., and Baralle, F. E. (1986) *EMBO J. 5*, 2825−2830.
7. Ingham, K. C., Brew, S. A., and Migliorini, M. M. (1989) *J. Biol. Chem. 264*, 16977−16980.
8. Bányai, L., Trexler, M., Koncz, S., Gyenes, M., Sipos, G., and Patthy, L. (1990) *Eur. J. Biochem. 193*, 801−806.
9. Bányai, L., and Patthy, L. (1991) *FEBS Lett. 282*, 23−25.
10. Skorstengaard, K., Holtet, T. L., Etzerodt, M., and Thorgersen, H. C. (1994) *FEBS Lett. 343*, 47−50.
11. Wilhelm, S. M., Collier, I. E., Marmer, B. L., Eisen, A. Z., Grant, G. A., and Goldberg, G. I. (1989) *J. Biol. Chem. 264*, 17213−17221.
12. Collier, I. E., Krasnov, P. A., Strongin, A. Y., Birkedal-Hansen, H., and Goldberg, G. I. (1992) *J. Biol. Chem. 267*, 6776−6781.
13. Bányai, L., Tordai, H., and Patthy, L. (1994) *Biochem. J. 298*, 403−407.
14. Murphy, G., Ngyen, Q., Cockett, M. I., Atkinson, S. J., Allan, J. A., Knight, C. G., Willenbrock, F., and Docherty, A. J. P. (1994) *J. Biol. Chem. 269*, 6632−6636.
15. Allan, J. A., Docherty, A. J. P., Barker, P. J., Huskisson, N. S., Reynolds, J. J., and Murphy, G. (1995) *Biochem. J. 309*, 299−306.
16. Constantine, K. L., Madrid, M., Bányai, L., Trexler, M., Patthy, L., and Llinas, M. (1992) *J. Mol. Biol. 223*, 281−298.
17. Pickford, A. R., Potts, J. R., Bright, J. R., Phan, I., and Campbell, I. D. (1997) *Structure 5*, 359−370.
18. Sticht, H., Pickford, A. R., Potts, J. R., and Campbell, I. D. (1998) *J. Mol. Biol. 276*, 177−187.
19. Briknarová, K., Grishaev, A., Bányai, L., Tordai, H., Patthy, L., and Llinás, M. (1999) *Structure 7*, 1235−1245.
20. Morgunova, E., Tuuttila, A., Bergmann, U., Isupov, M., Lindqvist, Y., Schneider, G., and Tryggvason, K. (1999) *Science 284*, 1667−1670.
21. Tjandra, N., and Bax, A. (1997) *Science 278*, 1111−1114.
22. Fischer, M. W. F., Losonczi, J. A., Weaver, J. L., and Prestegard, J. H. (1999) *Biochemistry 38*, 9013−9022.
23. Tolman, J. R., Flanagan, J. M., Kennedy, M. A., and Prestegard, J. H. (1995) *Proc. Natl. Acad. Sci. U.S.A. 92*, 9279−9283.
24. Tjandra, N., Grzesiek, S., and Bax, A. (1996) *J. Am. Chem. Soc. 118*, 6264−6272.
25. Bruschweiler, R., Liao, X. B., and Wright, P. E. (1995) *Science 268*, 886−889.
26. Tjandra, N., Garrett, D. S., Gronenborn, A. M., Bax, A., and Clore, G. M. (1997) *Nat. Struct. Biol. 4*, 443−449.
27. Fushman, D., Xu, R., and Cowburn, D. (1999) *Biochemistry 38*, 10225−10230.
28. Bright, J. R., Pickford, A. R., Potts, J. R., and Campbell, I. D. (1999) in *Methods in Molecular Biology*, Humana Press, Totowa, NJ.
29. Kay, L. E., Keifer, P., and Saarinen, T. (1992) *J. Am. Chem. Soc. 114*, 10663−10665.
30. Shaka, A. J., Barker, P. B., and Freeman, R. (1985) *J. Magn. Reson. 64*, 547−552.
31. Davis, D. G., and Bax, A. (1985) *J. Am. Chem. Soc. 107*, 2820−2821.
32. Kumar, A., Ernst, R. R., and Wüthrich, K. (1980) *Biochem. Biophys. Res. Commun. 95*, 1−6.
33. Zhang, O., Kay, L. E., Olivier, J. P., and Forman-Kay, J. D. (1994) *J. Biomol. NMR 4*, 845−858.
34. Farrow, N. A., Muhandiram, R., Singer, A. U., Pascal, S. M., Kay, C. M., Gish, G., Shoelson, S. E., Pawson, T., Forman-Kay, J. D., and Kay, L. E. (1994) *Biochemistry 33*, 5984−6003.
35. Boyd, J., Hommel, U., and Campbell, I. D. (1990) *Chem. Phys. Lett. 175*, 477−482.
36. Kay, L. E., Nicholson, L. K., Delaglio, F., Bax, A., and Torchia, D. A. (1992) *J. Magn. Reson. 97*, 359−375.
37. Wang, A. C., and Bax, A. (1993) *J. Biomol. NMR 3*, 715−720.
38. Palmer, A. G., Cavanagh, J., Wright, P. E., and Rance, M. (1991) *J. Magn. Reson. 93*, 151−170.
39. Tjandra, N., Szabo, A., and Bax, A. (1996) *J. Am. Chem. Soc. 118*, 6986−6991.
40. Palmer, A. G., Rance, M., and Wright, P. E. (1991) *J. Am. Chem. Soc. 113*, 4371−4380.
41. Mandel, A. M., Akke, M., and Palmer, A. G. (1995) *J. Mol. Biol. 246*, 144−163.
42. Boyd, J., and Redfield, C. (1998) *J. Am. Chem. Soc. 120*, 9692−9693.
43. Woessner, D. E. (1962) *J. Chem. Phys. 37*, 647−654.
44. Press, W. H., Flannery, B. P., Teukosky, S. A., and Vetterling, W. T. (1990) *Numerical Recipes*, 2nd ed., Cambridge University Press, New York.
45. Gosser, Y. Q., Zheng, J., Overduin, M., Mayer, B. J., and Cowburn, D. (1995) *Structure 3*, 1075−1086.
46. Improta, S., Krueger, J. K., Gautel, M., Atkinson, R. A., Lefevre, J.-F., Moulton, S., Trewhella, J., and Pastore, A. (1998) *J. Mol. Biol. 284*, 761−777.
47. Hashimoto, Y., Smith, S. P., Pickford, A. R., Bocquier, A. A., Campbell, I. D., and Werner, J. W. (2000) *J. Biomol. NMR* (in press).
48. Spitzfaden, C., Grant, R. P., Mardon, H. J., and Campbell, I. D. (1997) *J. Mol. Biol. 265*, 565−579.
49. Copie, V., Tomita, Y., Akiyama, S. K., Aota, S., Yamada, K. M., Venable, R. M., Pastor, R. W., Krueger, S., and Torchia, D. A. (1998) *J. Mol. Biol. 277*, 663−682.
50. Barbato, G., Ikura, M., Kay, L. E., Pastor, R. W., and Bax, A. (1992) *Biochemistry 31*, 5269−5278.
51. Hansen, A. P., Petros, A. M., Meadows, R. P., and Fesik, S. W. (1994) *Biochemistry 33*, 15418−15424.
52. Tjandra, N., Kuboniwa, H., Ren, H., and Bax, A. (1995) *Eur. J. Biochem. 230*, 1014−1024.
53. Lee, B. M., DeGuzman, R. N., Turner, B. G., Tjandra, N., and Summers, M. F. (1998) *J. Mol. Biol. 279*, 633−649.
54. Potts, J. R., Bright, J. R., Bolton, D., Pickford, A. R., and Campbell, I. D. (1999) *Biochemistry 38*, 8304−8312.
55. Bocquier, A. A., Potts, J. R., Pickford, A. R., and Campbell, I. D. (1999) *Structure 7*, 1451−1460.
56. Tjandra, N., Feller, S. E., Pastor, R. W., and Bax, A. (1995) *J. Am. Chem. Soc. 117*, 12562−12566.
57. Grant, R. P., Spitzfaden, C., Altroff, H., Campbell, I. D., and Mardon, H. J. (1997) *J. Biol. Chem. 272*, 6159−6166.
58. Lipari, G., and Szabo, A. (1982) *J. Am. Chem. Soc. 104*, 4546−4559.
59. Koradi, R., Billeter, M., and Wuthrich, K. (1996) *J. Mol. Graphics 14*, 51−59.

BI000427I